(16) DA-4-A-161102-B-52-E

(6) HIGH-VELOCITY FRAGMENT PENETRATION INTO SAND:
A COMPARISON OF EXPERIMENTAL RESULTS WITH
THEORETICAL PREDICTIONS.

(10) DWAIN K. BUTLER

(11) 1976

USAE WATERWAYS EXPERIMENT STATION
VICKSBURG, MISS. 39180

(12) 15p.

(17) 4-H-161102-B-52-E-04

INTRODUCTION

Research at the U. S. Army Engineer Waterways Experiment Station (WES) in penetration of high-velocity fragments into earth materials began in 1970 for the purpose of assessing the effectiveness of soil as a fortification material. The effort has consisted of a coupled analytical and experimental approach.[1-3] The experimental program has included the construction of a high-velocity powder gun capable of achieving impact velocities up to 0.274 cm/μsec (microsecond) (9000 ft/sec) for nominal 3-g fragments, and penetration tests of fragment-simulating projectiles into controlled soil targets.

Figure 1 illustrates the penetration depth-impact velocity behavior (over the velocity range of interest) for a hypothetical fragment and target material. There has been considerable experimental study in the low impact velocity range OA for penetration into soils, for which an increasing penetration depth with increasing impact velocity is observed. The data presented in Reference 2 cover the velocity range ABB'C. Curve ABC illustrates the

Figure 1. Penetration depth-impact velocity behavior for small fragments into earth media
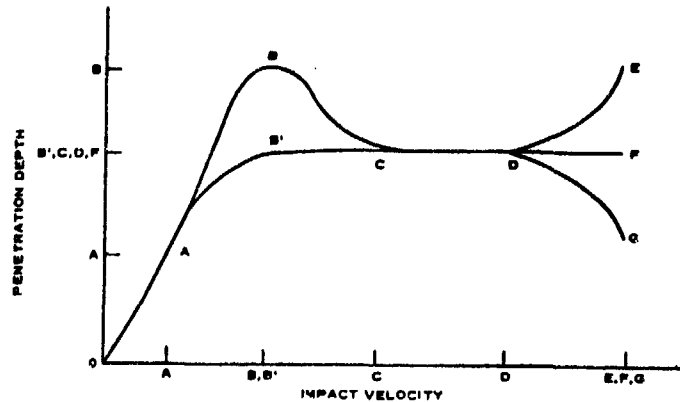
BUTLER

observed behavior of steel fragments penetrating sand, and curve AB'C
illustrates the observed behavior of steel fragments penetrating clay
(behavior believed to be due to fragment frontal enlargement). Pen-
etration tests (primarily into sand) in the velocity range CDEFG
have been conducted at only a few selected impact velocities with a
variety of fragment sizes and shapes, and thus it is not possible to
deduce the shape of the curve in this velocity range due to the ex-
tremely limited experimental data base. It is clearly important
with regard to the design of soil fortifications to define the pene-
tration depth-impact velocity curve in the velocity range CDEFG.

EXPERIMENTAL PROGRAM

Description of Test Program

The experimental program discussed in this report consisted
of 25 fragment penetration tests into dense sand targets. Data col-
lected from each test consisted of impact velocity, depth of pene-
tration, initial and final fragment dimensions, initial and final
fragment masses, sand target density, and grain-size analyses before
and after the penetration event. The high-velocity powder gun used
in the tests is documented in Reference 3.

Dense sand targets. A fine sand, known locally as Cook's
Bayou sand, was used for the targets. This sand is well documented
and was used as a target material, in both loose and dense states,
in an extensive series of penetration tests reported in Reference 2.
A target preparation procedure was followed which consistently pro-
duced targets with densities in the range 1.66 to 1.76 g/cm^3.

Fragments. Right-circular cylindrical
fragments were used in the study. Stress-strain
diagrams for the
two steels, a "soft"
steel (SS) and a
"hard" steel (HS),
are shown in
Figure 2 (static

Figure 2. Results
of unconfined com-
pression tests of
steel fragments
used in the test
program

Steel Projectile
(SAE 1020;
Designated SS)

Steel Projectile
(AISI C-1141;
Designated HS)

2
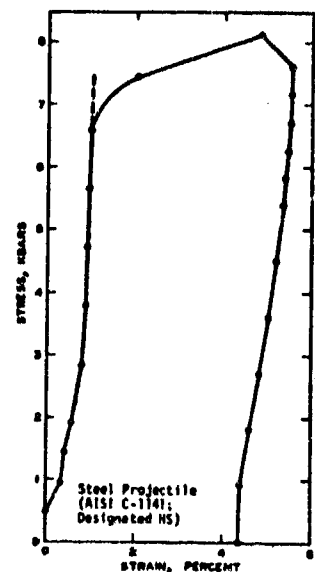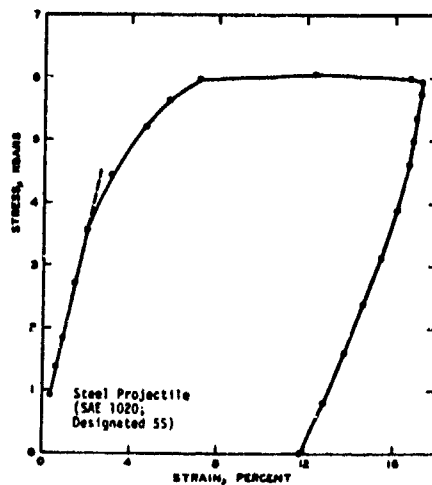
unconfined compression tests). Pertinent properties for the two
fragment materials used in the study are listed in the tabulation
below.

Metal	Length L, cm	Diam D, cm	Mass M, g	Density g/cm^3	Yield Strength σ_Y, Mbar	Brinell Hardness Number
Steel (SAE 1020)	0.80	0.787	3.00	7.71	0.0035	160
Steel (AISI C-1141)	0.78	0.78	2.87	7.70	0.0068	252

Test Results

The test results
are presented in Fig-
ures 3-5 and include
penetration depth,
frontal area enlarge-
ment coefficient C_A,
and reduced mass coef-
ficient C_M versus im-
pact velocity. The

Figure 3. Projectile
penetration into dense
sand
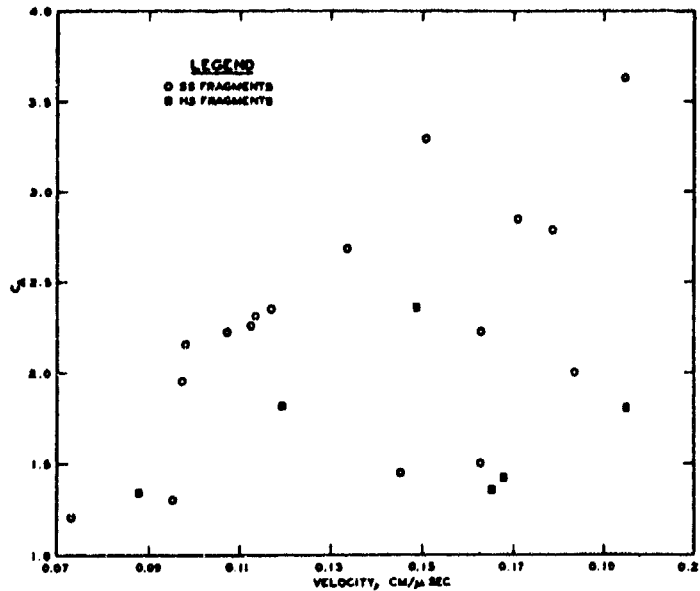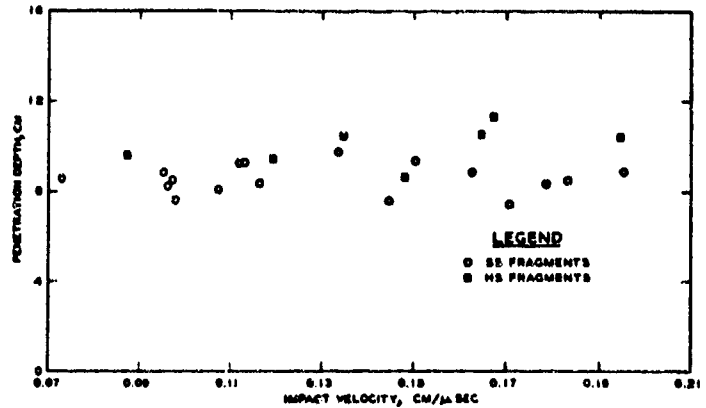

Figure 4. Frontal area
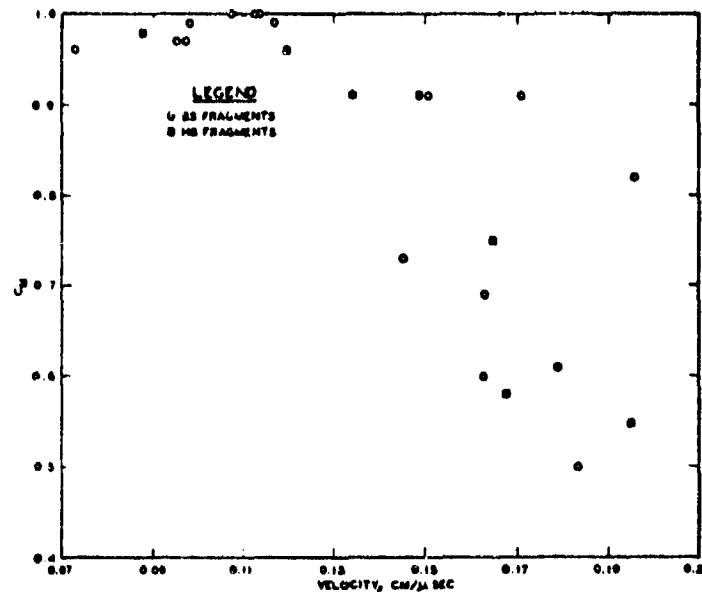enlargement coefficient
versus impact velocity

Figure 5. Reduced mass coefficient versus impact velocity

coefficients C_A and C_M define the enlargement of the frontal area of the fragment due to plastic deformation and the loss of mass due to erosion, respectively. $C_A = A_f/A_i$ and $C_M = M_f/M_i$, where A_f = frontal area of fragment after penetration event, A_i = initial frontal area, M_f = mass of projectile after penetration event, and M_i = initial mass.

ANALYSIS AND DISCUSSION OF EXPERIMENTAL PROGRAM

Projectile Penetration Depth, Deformation, and Mass Loss

   Analysis of results. It is evident from Figures 4 and 5 that the fragments did not penetrate as rigid bodies of constant mass in any of the penetration tests conducted. In all cases, the fragments deformed, and in all but three cases, mass was lost during the event. Figure 6 illustrates the typical appearance of the HS fragments following penetration into the dense sand. It was concluded in Reference 2 that, in the rigid penetration range in which the fragments undergo only elastic deformations and no mass loss, the depth of penetration is independent of the yield strength of the material composing the fragment and that penetration depth increases continuously with increasing impact velocity. The data presented in Reference 2 indicate that the rigid penetration range for steel fragments (same material as the HS fragments in the study reported here) terminates at impact velocities of 0.0762 to 0.0914 cm/μsec (2500 to 3000 fps) in dense sand. Thus, the range of impact velocities in this study is above the rigid penetration range.

4

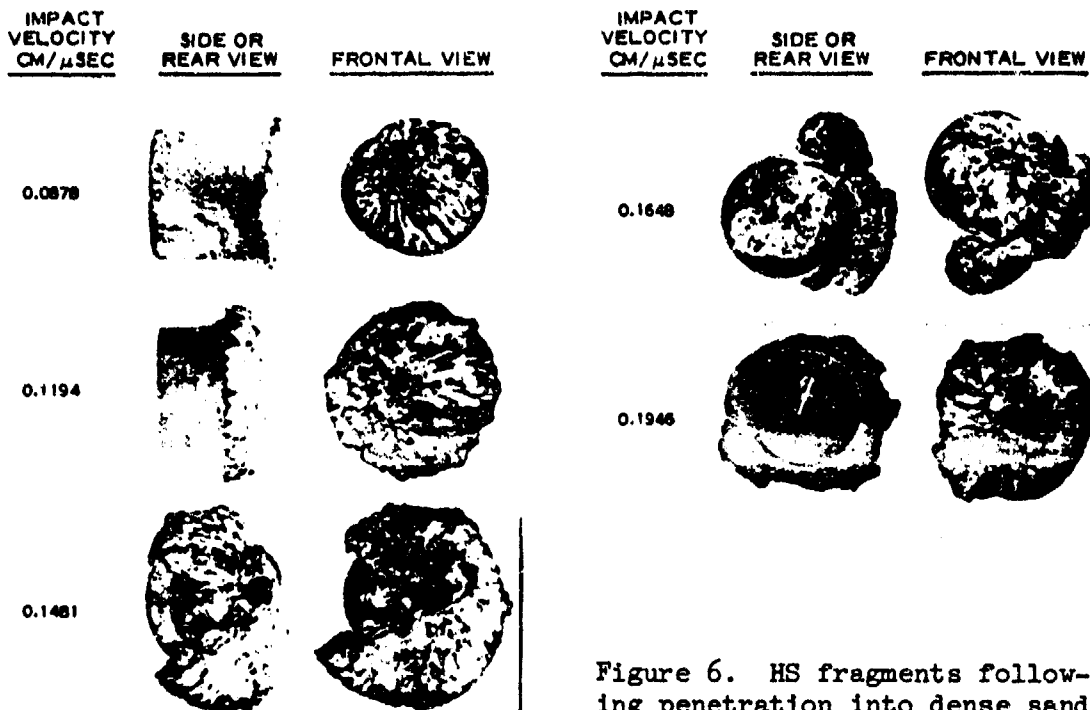| IMPACT VELOCITY CM/μSEC	SIDE OR REAR VIEW	FRONTAL VIEW	IMPACT VELOCITY CM/μSEC	SIDE OR REAR VIEW	FRONTAL VIEW
0.0878			0.1648		
0.1194			0.1946		
0.1481					

Figure 6. HS fragments following penetration into dense sand

Penetration depths achieved by the SS fragments appear to be slightly smaller over the investigated impact velocity range than those for the HS fragments. The data for the SS fragments are scattered about a constant penetration depth of about 8.6 cm. Figure 7 compares the data from Reference 2 for dense sand penetration with data from the tests in this study for HS fragments. The data from the tests in this study correlate quite well with the higher velocity data from Reference 2 and thus appear to form a logical extension for the dense sand penetration of this type steel (HS) fragment to impact velocities of 0.20 cm/μsec (6500 fps). It is demonstrated in Reference 4 that, for long rod penetration, it is theoretically possible to have a decrease in penetration depth with increasing impact velocity as in Figure 7. It is interesting to note that the general shape of the penetration versus impact velocity curve (say a best-fit curve to the data) of Figure 7 closely resembles the curves of Reference 4 for cases in which the strength of the target is less than the strength of the fragment.

Phenomenological discussion. Following impact, plane shock waves propagate into the target and fragment with magnitudes which depend on the impact velocity and the material properties of the target and fragment. The plane shocks are quickly distorted and
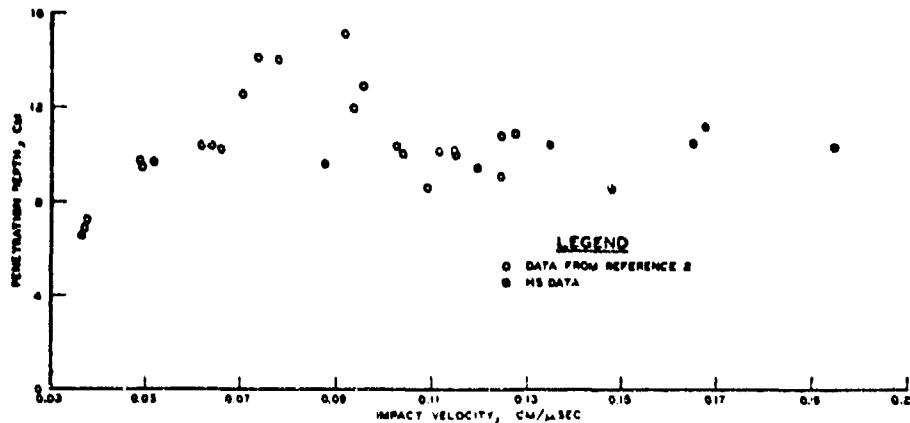
Figure 7. Comparison of data from Reference 2 with data for HS fragments in this study penetrating dense sand

attenuated due to rarefaction waves from lateral and rear surfaces of the fragment and from the "free" surface of the target. The rarefaction waves from the lateral fragment surface will generate tensile stresses in the fragment which, if the dynamic yield strength of the fragment material is exceeded, will tend to cause plastic deformations and lateral material flow (radial flow). It is this mechanism which produces the familiar, characteristic mushroom shapes shown in Figure 6.

Thus, as impact velocity increases above a critical velocity (the impact velocity for which stresses in the fragment exceed the yield stress), plastic flow will occur and continue until stresses fall below the yield stress (which itself may have changed during the event). At high impact velocities, the frontal area will not only increase but the fragment will lose mass as the "mushrooming" material separates. For impact and penetration into sand, mass is also lost due to the abrasive action of the sand grains on the fragment, and this effect should increase in importance as the impact velocity increases and as the yield strength and hardness of the material composing the fragment decrease.

In general, the penetration depth depends directly on the fragment mass and inversely on the presented frontal area (perhaps to some power). The diagrams in Figure 8 illustrate in section view the geometries of the recovered fragments for increasing impact velocity. It is hypothesized that the diagrams can also be considered as a time sequence of events in the penetration process for an impact velocity $V_6 > V_c$, where the dashed lines in Figure 8d represent incipient separation of the "mushrooming" material. Figure 9 presents hypothetical plots of C_A and C_M versus impact velocity.

Figure 8. Cross-sectional views of fragments following penetration at increasing impact velocities V_i (V_c = critical impact velocity for plastic flow)
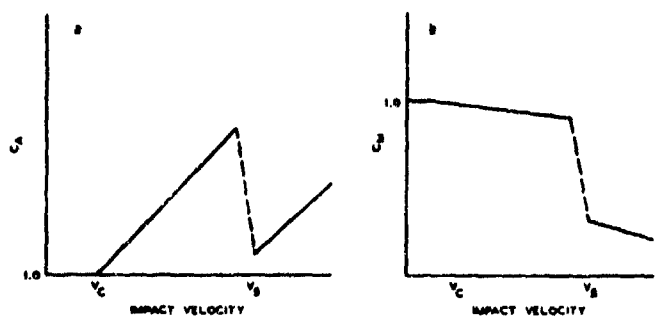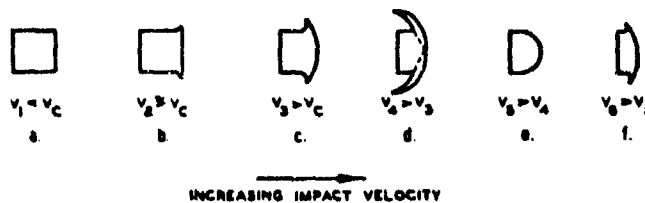

INCREASING IMPACT VELOCITY

Figure 9. Hypothetical plots of C_A and C_M versus impact velocity for the phenomena represented in Figure 8

C_A remains constant at 1.0 until V_c is exceeded and then increases in some monotonic manner until a velocity V_5 is reached, at which point the separation indicated in Figures 8d and 8e occurs with a sudden drop in C_A . At some low velocity (not necessarily V_c), mass begins to be lost due to erosion and continues throughout the impact velocity range. The sudden drop in C_M at V_5 again corresponds to the separation indicated in Figures 8d and 8e.

  Recovered steel from both type fragments contained rather large curved platelike pieces indicative of the mechanism proposed in Figure 8d. In general, the pieces of the SS fragments were larger than those of the HS fragments, as would be expected due to the lower yield strength and greater ductility of the SS material. Also, the edges of the HS fragments were drawn thinner and had a more jagged, striated appearance (this effect might be indicative of strain hardening; see Figure 2). Very small pieces of the fragments such as might result from the abrasive action of the sand were present following the tests. Evidences of high temperatures during the penetration process were the "charred" appearance of the fragments and a noticeable elevation in temperature of large volumes of the target. Also present in the recovered pieces of the HS fragments were grayish-black spherules (≤ 1 mm in diameter) which could have been formed only by complete melting. An X-ray diffractogram revealed that the spherules contained α-iron and quartz. Also, the diffractogram contained a broad maximum, characteristic of an amorphous solid, and an intriguing possibility is that the maximum could be an indication of the presence of elemental silicon in an

7

amorphous form. This possibility is suggested by the presence of iron oxide on some of the steel fragments. Thus, it is possible that the penetration process provided the extreme reducing environment necessary for the reaction $Fe_3O_4 + 2Si \rightarrow 3Fe + 2SiO_2$ to occur in the reverse direction (5).

Sand Comminution and Grain-Size Analyses

Comminution (crushing) of sand grains has commonly been observed in standard laboratory testing of sands (6,7). Application of confining pressures (isotropic compression) above a threshold value results in a shift of the grain-size distribution (gradation) curve of a test sample. At a given confining pressure, application of shearing stresses results in a further and relatively larger upward shift in the grain-size distribution curve. Sand comminution has also been observed in fragment penetration tests and considered in analyses of penetration tests into sand (8-11). For a given fragment, a minimum impact velocity exists below which sand comminution does not occur to a significant extent (8,10). Thompson (11, has observed the formation of "sand cones" on the noses of projectiles with blunt, hemispherical, and ogival nose geometries. The sand cone is formed of compacted, comminuted sand which adheres to the fragment and moves through the target media as part of the fragment once it has formed. Some evidence of sand cone formation was present on a few of the recovered fragments, but in none of the cases was a "complete" 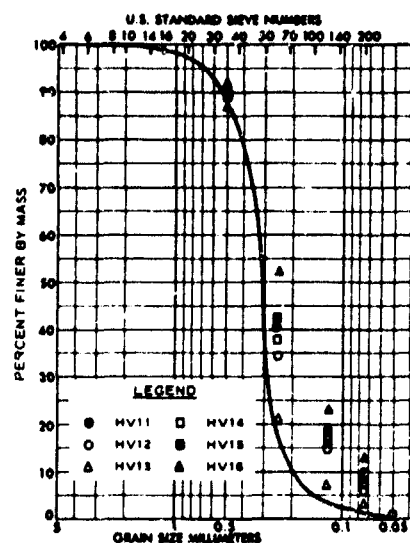sand cone observed or recovered as discussed by Thompson (11) for larger diameter projectiles. It is possible that the complex mass loss and frontal enlargement mechanisms, proposed earlier for the small blunt fragments used in these tests, prevented the formation of other than temporary sand cones. The comminution process is undoubtedly very complex for the fragment penetration case (consisting of comminution caused by the initial shock wave, abrasion between grains caused by shearing motions as the sand is pushed aside, abrasion caused by contact between individual grains and the fragment itself, etc.).

Figure 10 presents typical grain-size analysis results for the comminuted sand material obtained from the fragment tracks following the tests. The figure contains the curve for the parent material, and the data for each test (for

Figure 10. Grain-size data for test Nos. HS-DS-HV11 to -HV16

each grain size) are indi-
cated by different symbols.
In order to illustrate more
explicitly the effect of im-
pact velocity on grain-size
distribution, the percent
finer by mass data for three
selected grain sizes (0.25,
0.125, and 0.074 mm) versus
impact velocity are plotted
in Figures 11 and 12 for
the SS and HS fragment tests,
respectively. The points on
the percent finer axis for
zero impact velocity are for
the parent material. A large
jump in the percent finer by
mass values is evident in
Figure 12 at an impact veloc-
ity of about 0.10 cm/μsec.
It is significant to note
that this is about the veloc-
ity at which the dramatic de-
crease in penetration depth
occurs in the composite data
plot in Figure 7 and also
about the velocity at which a
significant increase in the
frontal enlargement coeffi-
cient is observed (Reference 2
and Figure 4). The data in
Figures 11 and 12 are consis-
tent with the concept that
comminution does not occur
below a minimum impact veloc-
ity. It is tempting, but
would be too much a matter of
conjecture at this point, to
interpret each of the in-
creases and decreases in the
percent finer versus impact
velocity data in Figures 11
and 12 in terms of the mecha-
nism proposed in Figures 8
and 9 and the C_A and C_M
data in Figures 4 and 5. If

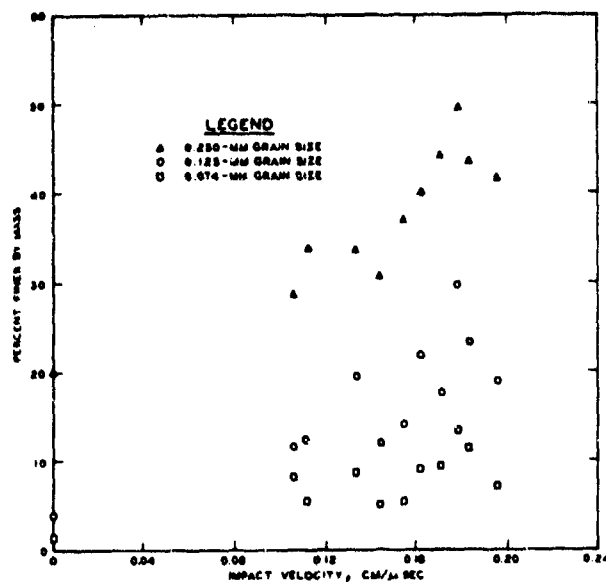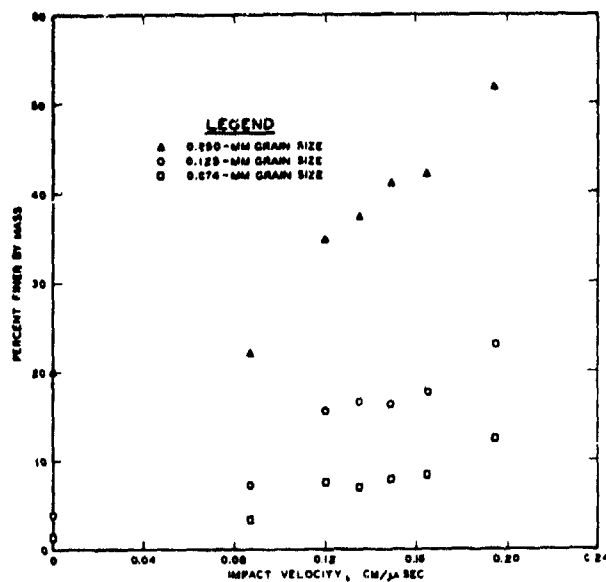

Figure 11. SS fragment tests

Figure 12. HS fragment tests

9

such an interpretation can be further substantiated, it will represent a significant advancement in the understanding of the energy exchange mechanisms operating during the impact and penetration process.

Dynamic Yield Strengths of Fragment
Materials and Energy Partitioning Considerations

Taylor (12) has demonstrated that the profile of a cylindrical rod following impact with a <u>rigid</u> boundary can be related to the dynamic yield strength of the material composing the rod. In a more recent study, Wilkins (13), based on the method proposed by Taylor, simulated the impact of rods, of several material types and length-to-diameter ratios varying from 1 to 15, into a <u>rigid</u> boundary with an elastic-plastic finite difference computer code. He also conducted experimental impact tests and demonstrated that the observed rod profile after impact for a given impact velocity can be duplicated in the code calculations by varying the yield strength parameter; then, using the yield strength parameter for which the profile has been duplicated, the profiles following impact at different impact velocities can also be duplicated. The yield strengths deduced by this procedure agree quite well with previously published values determined by plane shock wave experiments (14,15) and rod penetration tests (16). Butler (17) has demonstrated that measurements of fragment deformations, following <u>penetration</u> into an explosive simulant material, can be used to deduce the dynamic yield strength of a fragment. Using pressure versus relative density relations such as found in References 2, 3, 9, and 18, a computer code based on the method of characteristics was used to solve the one-dimensional analogy of the fragment-target impact to obtain the impact pressure-impact velocity and particle velocity-impact velocity relations shown in Figure 13.
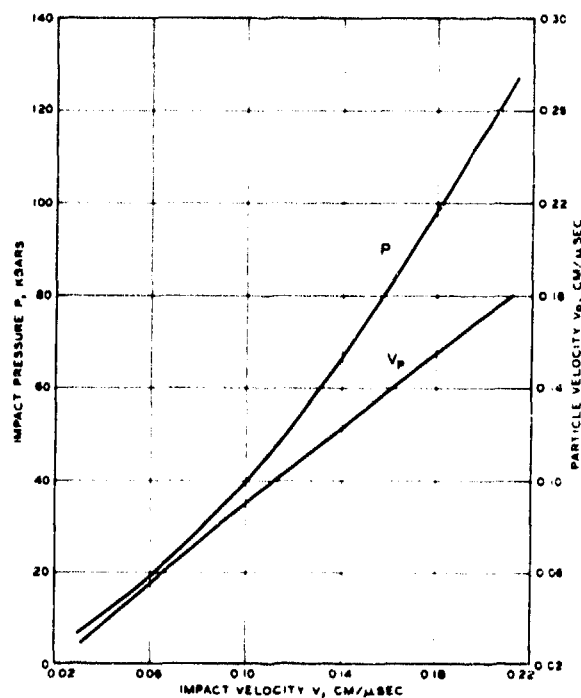

Figure 13. Impact pressure and particle velocity in target versus impact velocity

Based on the data presented in Reference 2 and in Figure 4, critical impact velocities for deformation of the HS and SS fragments were estimated to be 0.07 and 0.042 cm/μsec, respectively. From Figure 13, the code calculations for these impact velocities give 18 and 11 kbars for the dynamic strengths of the HS and SS materials, respectively. The dynamic strength value of 11 kbars for the SS fragment material (SAE 1020 steel) correlates quite well with dynamic yield strength values of 12.8 and 10.4 kbars for two thicknesses of SAE 1020 steel reported in Reference 14. There are no dynamic strength data available for the HS fragment material (AISI C-1141), however it is possible to infer a dynamic strength value for the HS material from published values for SAE 4340 and SAE 1040 steels which is in reasonable agreement with the value determined here (3). Additional credence to the impact pressures computed by the characteristics code using the one-dimensional analogy is given by experimental data such as presented in Reference 19.

With the particle velocities calculated for the fragment and target at impact (see Figure 13), it is possible to calculate the initial energy partitioning at the time when the shock wave reaches the rear of the fragment as a function of impact velocity based on the one-dimensional considerations of Gault and Heitowit (20). The results of this type analysis for the cases presented in this report are given in Reference 3. While the results of such an analysis are valid only for the initial energy partition at impact, they qualitatively confirm many of the phenomenological observations of the experimental program. For example, the predicted increasing percentage of energy transferred to the target as internal energy with increasing impact velocity is consistent with and accounts for the increased sand comminution observed as the impact velocity increases. Also, the observed elevated temperatures in the target at the higher impact velocities are consistent with the increasing percentages of energy transferred to internal energy of the fragment and target. The increasing percentage of energy transferred to internal energy of the fragment raises the temperature and serves as a driving mechanism for the material flow discussed earlier (3).

Correlation of Experimental Results
with Penetration Model Predictions

Rohani (2) correlated his experimental results with the prediction of an analytical penetration model. The model is based on an analogy with the dynamic expansion of a spherical cavity and has been extended by WES to treat arbitrary fragment nose shapes, to treat layered targets, and to use a complete pressure-density relation for the target (21). He concluded that the WES penetration model could be used to predict or reasonably bound the penetration

depths of high-velocity fragments into soil targets. On this basis, the penetration model was used in an attempt to duplicate the experimental results of Figures 3 and 7 and to investigate the feasibility of bounding the penetration depths.

For the penetration model calculations, the initial target densities, the pressure versus relative density relation for sand (2,3), and the values of Young's modulus, strain-hardening modulus, and yield strength recommended by Rohani (Table 7, Reference 2) for the dense sand targets were used to characterize the targets. The fragments were characterized by their mass, presented frontal area, and a function describing their nose shape. For an upper-bound calculation, it seemed appropriate to use the initial mass M_i and the initial frontal area A_i ; for the lower-bound calculation, it was assumed that all deformation and mass loss would occur at the instant of impact, and the final mass M_f and final frontal area A_f were used for the calculation. Assuming a hemispherical nose shape results in a higher upper-bound estimate than that obtained by assuming a blunt nose shape. For the lower-bound estimates, the assumption of a hemispherical nose is consistent with the observed deformed shape of the recovered fragments. Correlations of the experimental penetration results for SS and HS fragments with upper- and lower-bound penetration model calculations are presented in Figures 14 and 15, respectively.

In all cases, the experimental penetration depths from these tests are bounded by the penetration model upper- and lower-bound estimates. In fact, in most of the cases the experimental value is approximated by the mean of the upper- and lower-bound estimates. This trend is indicative of the fact that the physical mechanisms actually occurring (perhaps as proposed in Figure 8) are intermediate to the extreme assumptions used to make the upper- and lower-bound estimates. The data from Reference 2 in Figure 15 are not
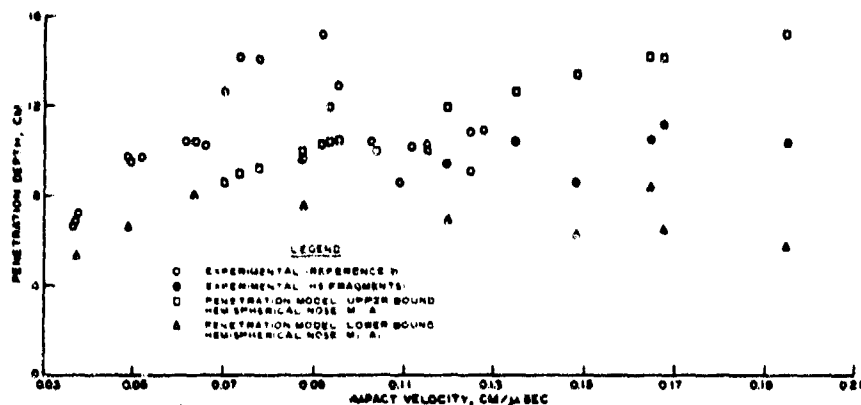
Figure 14.   SS fragments
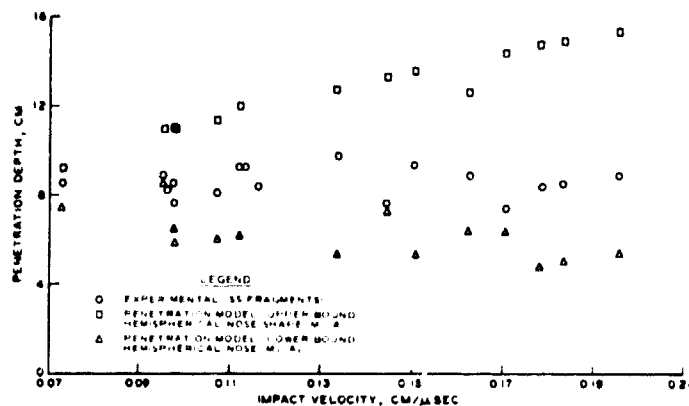
Figure 15. HS fragments

bounded by the upper-bound penetration model calculations. It was
demonstrated in a parameter study in Reference 2, however, that the
dense sand penetration values could be bounded by a different (and
perhaps better) selection of target material properties for use in
the model calculations.

CONCLUSIONS

The results of 25 penetration tests of cylindrical fragments
into dense sand targets are presented. The following conclusions
and observations are based on these results:

<u>a.</u> Dense sand is an effective medium for stopping high-
velocity projectiles or fragments.

<u>b.</u> The penetration depth attained by high-velocity projec-
tiles or fragments in dense sand is not a monotonically increasing
function of impact velocity but tends to remain constant after a
critical impact velocity* is exceeded. The critical impact velocity
increases as the strength of the fragment material increases. The
overall shape of the penetration depth versus impact velocity curve
depends in a very complex manner on the details of fragment deforma-
tion and mass loss during penetration.

<u>c.</u> With reference to Figure 1, the data of this report and
Reference 2 demonstrate that the behavior indicated by curve CDE
does not occur for the types of steel fragments tested. Although
the desired maximum impact velocity of 0.274 cm/μsec (9000 fps) was
not achieved in this study, the observations of penetration depth
and fragment mass loss and deformation (at impact velocities up to

---

* Velocity at which deformation of the fragment is initiated.

BUTLER

0.2 cm/µsec) suggest that the constant penetration depth represented
by curve CDF in Figure 1 is an upper bound for the penetration depths
which would be observed at higher impact velocities (>0.2 cm/µsec).

    <u>d</u>. Sand grain comminution occurring during penetration is
reflected in an upward shift of the gradation curves, with increas-
ing impact velocity, relative to the gradation curve of the parent
material. The percent finer by mass data for the HS fragments (Fig-
ure 12) indicate a jump in value at about the same impact velocity
as the critical velocity for the HS material discussed in sub-
paragraph <u>b</u> above. This increase indicates a jump in the energy
being transferred to the comminution process at this velocity.

    <u>e</u>. A one-dimensional analogy of the fragment penetration
process gives reliable values for the impact pressures and particle
velocities.

    <u>f</u>. The WES penetration model can be used to bound the pene-
tration depths of small projectiles and fragments in dense sand.

ACKNOWLEDGMENT

REFERENCES

1. Reeves, G. N., Rohani, B., "Fragment and Projectile Penetration
    Resistance of Soils; Literature Review and Preliminary Theoreti-
    cal Study of Soils as a Fortification Material," MP S-71-12,
    Rpt 1, Jul 1971, USAEWES, Vicksburg, Miss.
2. Rohani, B., "Fragment and Projectile Penetration Resistance of
    Soils; High-Velocity Fragment Penetration into Laboratory-
    Prepared Soil Targets," MP S-71-12, Rpt 2, Jun 1973, USAEWES,
    Vicksburg, Miss.
3. Butler, D. K., "Development of a High-Velocity Powder Gun and
    Analysis of Fragment Penetration Tests into Sand," MP S-75-27,
    Oct 1975, USAEWES, Vicksburg, Miss.
4. Tate, A., "Further Results in the Theory of Long Rod Penetra-
    tion," <u>Jour, Mech and Phys of Solids,</u> Vol 17, 1969.
5. Stacey, F., <u>Physics of the Earth,</u> Wiley, 1969.
6. Clough, G. W., <u>An Investigation of the Shear Strength of Sand
    at High Pressures,</u> MS Thesis, Ga. Inst of Tech, Oct 1964.

7. Vesic, A. S., Clough, G. W., "Behavior of Granular Materials Under High Stresses," Jour, Soil Mech and Foun Div, ASCE, May 1968.

8. Allen, W. A., Mayfield, E. B., Morrison, H. L., "Dynamics of a Projectile Penetrating Sand," Jour of Appl Phys, Vol 28, No. 3, Mar 1957.

9. Braslau, D., "Partitioning of Energy in Hypervelocity Impact Against Loose Sand Targets," Jour of Geophys Res, Vol 75, No. 20, Jul 1970.

10. Hakala, W. W., Resistance of a Granular Medium to Normal Impact of a Rigid Projectile, PhD Dissertation, Va. Polytech Inst, Jun 1965

11. Thompson, L. J., "Dynamic Penetration of Selected Projectiles into Particulate Media," Development Rpt SC-DR-66-376, 1966, Sandia Corporation, Albuquerque, N. Mex.

12. Taylor, G. I., "The Use of Flat-Ended Projectiles for Determining Dynamic Yield Stress," Proc of the Royal Soc, Vol 194A, Sep 1948.

13. Wilkins, M. L., Guinan, M. W., "Impact of Cylinders on a Rigid Boundary," Jour of Appl Phys, Vol 44, No. 3, Mar 1973.

14. Jones, O. E., Nielson, F. W., Benedict, W. B., "Dynamic Yield Behavior of Explosively Loaded Metals Determined by a Quartz Transducer Technique," Jour of Appl Phys, Vol 33, No. 11, Nov 1962.

15. Duvall, G. E., Response of Metals to High Velocity Deformation, Ed by P. W. Shweman and V. F. Zackay, Interscience, NY, 1961.

16. Tate, A., "A Theory for the Deceleration of Long Rods After Impact," Jour, Mech and Phys of Solids, Vol 15, pp 387-399, 1967.

17. Butler, D. K., "Analysis of Projectile Penetration into Aroclor," U. S. Naval Ordnance Laboratory, NOLTN8916, Jul 1970.

18. Van Thiel, M., Ed, Compendium of Shock Wave Data, Lawrence Radiation Laboratory, UCRL-50108 Vol 1, Supplement 1, Oct 1967.

19. Eichelberger, R. J., "Hypervelocity Impact," Behavior of Materials Under Dynamic Loading, Ed by N. J. Huffington, Jr., ASME, 1965.

20. Gault, D. E., Heitowit, E. C., "The Partition of Energy for Hypervelocity Impact Craters Formed in Rock," Proc of the Sixth Hypervelocity Impact Sym, Cleveland, Ohio, Vol II, Part 2, 1963.

21. Bernard, R. S., Hanagud, S. V., "Development of a Projectile Penetration Theory," TR S-75-9, Rpts 1 and 2, USAEWES, Vicksburg, Miss.